Intermetallics 98 (2018) 1–10

Contents lists available at ScienceDirect

Intermetallics

journal homepage: www.elsevier.com/locate/intermet

New clathrate-like compound $Eu_7Cu_{44}Sb_{23-\delta}$: synthesis, crystal and electronic structure, and the effect of As-for-Sb substitution on the magnetic properties

Igor V. Plokhikh[a,b,*], Dmitry O. Charkin[a], Alexey N. Kuznetsov[a,c], Valery Yu Verchenko[a,d], Ivan A. Ignatiev[a], Sergey M. Kazakov[a], Alexander A. Tsirlin[e], Andrei V. Shevelkov[a]

[a] Lomonosov Moscow State University, 119991, Moscow, Russia
[b] University of Regensburg, 93053, Regensburg, Germany
[c] Kurnakov Institute of General and Inorganic Chemistry RAS, 1991, Moscow, Russia
[d] National Institute of Chemical Physics and Biophysics, 12618, Tallinn, Estonia
[e] Experimental Physics VI, Center for Correlations and Magnetism, Institute of Physics, University of Augsburg, 86135, Augsburg, Germany

ARTICLE INFO

Keywords:
Intermetallics
Magnetic properties
Site occupancy
Electronic structure
Calculation
Diffraction/sacterring (electron, neutron and X–ray)

ABSTRACT

A new intermetallic compound, ternary antimonide $Eu_7Cu_{44}Sb_{23-\delta}$ [*Fm*-3m, a = 17.4346(1)Å, δ = 0.5(1)] is reported. The compound forms a continuous substitutional solid solution with its $Eu_7Cu_{44}As_{23}$ archetype. The gradual substitution of Sb for As evokes partial disorder in the copper–pnictogen framework that becomes more pronounced with an increase of the Sb content and changes magnetic properties. Whereas $Eu_7Cu_{44}As_{23}$ is metallic ferromagnet below 17 K, $Eu_7Cu_{44}Sb_{23-\delta}$ shows paramagnetic behavior down to 1.8 K according to the magnetic measurements, while retaining metallic properties according to the DFT calculations. The origin of the disorder, the structure-property relationships, as well as prospects of further substitution in the anionic sublattice are discussed.

1. Introduction

Despite being a rare-earth element, europium commonly behaves as an isolobal analog of alkaline earth metals, since it easily adopts the oxidation state of 2+, particularly in tetrelide, pnictide, and chalcogenide environment. The radius of Eu^{2+} is only slightly smaller than that of Sr^{2+} [1], thus facilitating the formation of isostructural compounds even when the crystal structure requires a precise size matching [2–5]. The ternary systems Eu-T-Pn (T – transition metal, Pn – pnictogen, P, As, Sb) host many peculiar compounds [6,7] including iron-based superconductors [8]. With 7 unpaired 4*f* electrons, Eu^{2+} cations possess high localized magnetic moments and tend to undergo long-range magnetic ordering at low temperatures. As a result, the majority of Eu^{2+}-bearing pnictides and chalcogenides behave as conventional paramagnets [9,10] or order antiferromagnetically with low T_N (below 50 K) [11]. The examples of high-T_N antiferromagnets or ferromagnets are yet rare [12–15]. Relatively high ordering temperatures are commonly associated with metallic conductivity, and it is fairly natural that conduction electrons amplify interactions between localized magnetic moments via the RKKY mechanism. This may be the case in the recently discovered compound $Eu_7Cu_{44}As_{23}$ (a $BaHg_{11}$ derivative, Fig. 1) that orders ferromagnetically below 17 K [16]. Sr^{2+} can substitute Eu^{2+} yielding non-magnetic metal $Sr_7Cu_{44}As_{23}$, whereas Ca^{2+} and Ba^{2+} do not form such a compound. Since $Eu_7Cu_{44}As_{23}$ is metallic and do not follow the Zintl-Klemm electron counting scheme, it was possible to further explore this structure type via partial substitution of Cu by Fe, Co, and particularly Ni [17]. While the bond distances are affected rather moderately, essential changes in the magnetic properties are observed. While Ni-substitution results in the increase of T_C even at moderate doping levels, Fe-substitution completely suppresses ferromagnetic ordering. However, the variation of the electron count occurs simultaneously with the variation of the Eu^{2+} – Eu^{2+} separation, which does not allow to trace the effects of these two factors separately.

In order to delineate the role of the Eu-Eu distances, we have undertaken an isovalent substitution of arsenic by antimony in the structure of the parent arsenide compound. This resulted in the discovery of a new compound, $Eu_7Cu_{44}Sb_{23-\delta}$. Moreover, we have found out that it formed a continuous $Eu_7Cu_{44}As_{23-x}Sb_x$ solid solution with the arsenide. Along with the structural analysis, electronic structure calculations as well as measurements of magnetic properties were performed and are reported in this paper.

* Corresponding author. University of Regensburg, 93053, Regensburg, Germany.
E-mail address: ig.plohih@yandex.ru (I.V. Plokhikh).

https://doi.org/10.1016/j.intermet.2018.04.005
Received 29 December 2017; Received in revised form 19 March 2018; Accepted 8 April 2018

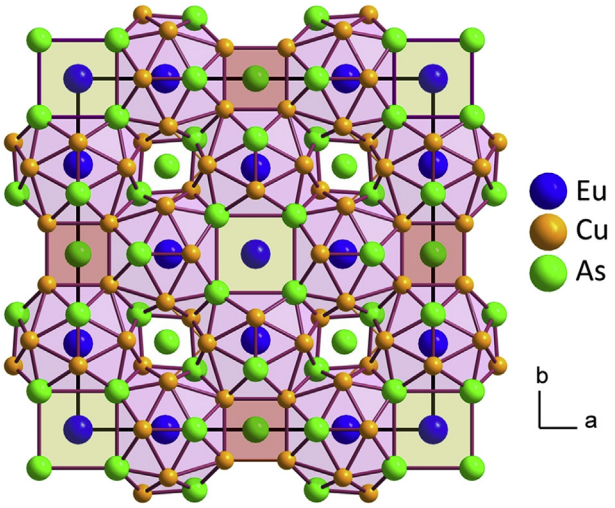

Fig. 1. A projection of the unit cell for $Eu_7Cu_{44}As_{23}$ along the 001 direction. Cell edges are outlined with thick black lines.

2. Experimental

Synthesis. The synthetic procedure for the solid solution was essentially the same as described for $A_7Cu_{44}As_{23}$ (A = Sr, Eu) [16,17]. Simple elements were used as starting materials. Powdered Cu (99.99% purity) was preheated in a hydrogen flow in order to remove surface oxides. Arsenic oxide was removed from powdered As (99.99% purity) by heating in a temperature gradient in an evacuated silica tube. Eu and Sr compact metals (99.5% purity) were chopped in Ar-filled glove box just before the preparation of the samples. Antimony (99.99% purity) was used as purchased. Stoichiometric mixtures with the total mass of about 1 g were pressed into pellets, sealed *in vacuo* (ca. 10^{-2} Torr) in silica tubes, and heated at 973–1023 K for 48 h. The annealed samples were thoroughly re-ground and re-annealed at the same temperature for 48 h until no changes were observed in their PXRD patterns. Phase composition was checked using the Bruker D8 Advance diffractometer ($CuK\alpha_{1,2}$ radiation); elemental composition was confirmed by EDX analysis using JEOL JSM 6490LV scanning electronic microscope.

Crystal structure refinement. Powder XRD data sets were collected on the Powder X'Pert^3 diffractometer ($CuK\alpha_{1,2}$ radiation, reflection geometry) from PANalytical, as well as at the ID22 beamline of the European Synchrotron Radiation Facility (ESRF) (λ = 0.35414 Å). For synchrotron measurements, samples were loaded into thin-walled borosilicate glass capillaries with the external diameter of 0.3 mm, and spun during the measurement. The signal was collected by 8 scintillation detectors each preceded by a Si(111) analyzer crystal. The PXRD data were processed in the JANA2006 software [18]. The structure of pristine $Eu_7Cu_{44}As_{23}$ [16] was used as a starting model. First, profile parameters as well as atomic coordinates were refined. The ratio of substituents was then refined while isotropic ADPs were fixed at 0.01 Å^2 for all atoms. Small amounts of impurities not detected upon routine phase analysis were included into the refinement if present. Finally, all parameters were refined simultaneously. Further refinement details and results are collected in Tables 1–3. Typical Rietveld plots are presented in Fig. 2.

Electronic structure calculations were performed on the DFT level using PAW pseudopotential approach as implemented in the VASP code [19,20]. Perdew-Burke-Ernzerhof exchange-correlation functional of the GGA-type was used in the calculations [21]. The calculations were performed on a 6 × 6 × 6 Monckhorst-Pack *k*-point mesh in the reciprocal space [22]. In order to minimize the effects from highly correlated 4*f* electrons of the Eu^{2+} ions on the states near the Fermi level, we utilized a special PAW pseudopotential for Eu^{2+}, supplied with the VASP package, where these electrons were considered as a part of the core. The energy cut-off was set at 400 eV. Atomic charges were estimated according to the R. Bader's QTAIM approach [23,24].

Thermodynamic and magnetic measurements. The DC magnetization of polycrystalline samples was measured with the VSM setup of a Physical Property Measurement System (PPMS, Quantum Design). The M(H) curves were obtained at 2 K and at 5 K by sweeping magnetic field from 0 T to 14 T. The DC susceptibility $\chi = M/H$ was measured in the temperature range 2–380 K in magnetic fields of 0.1 T, 0.5 T, 2 T, and 5 T. The heat capacity measurements were performed using a relaxation-type calorimeter provided with the Heat Capacity Option of PPMS (Quantum Design) in the temperature range of 1.8–2 K in $\mu_0 H = 0$ T and $\mu_0 H = 7$ T magnetic fields.

3. Results and discussion

Synthesis. Phase-pure $A_7Cu_{44}As_{23}$ (A = Sr, Eu) can be relatively easily prepared from the elements by several subsequent annealing steps at 1073 K [16,17]. In contrast, the synthesis of the Sb-substituted samples requires lower temperature and slightly longer annealing time. Phase-pure (or nearly so) samples of $A_7Cu_{44}As_{23-x}Sb_x$ (A = Sr, $x = 2$; A = Eu, $x = 4$, 5, 7, 10, 11, 15) can be prepared at 1023 K, while for $x = 19$, 20, 23 the optimal synthesis temperature is 973 K, leading to samples containing less than 5% of the non-magnetic Cu_2Sb admixture. Unlike that of the arsenides, the synthesis of antimony-containing samples is more sensitive to the choice of starting materials and requires particularly fine chopping of the starting mixtures of elements followed by their thorough homogenization, probably due to the competing formation of other kinetically stable compounds.

Table 1
Details of powder diffraction experiments for $Eu_7Cu_{44}As_{23-x}Sb_x$ solid solution with different *x*.

Sb content, *x*	4	5	10	15	20	23 (RT)	23 (80 K)	2 (Sr)
Space group				Fm-3m				
Z				4				
				Cell parameters:				
a, Å	16.8047(1)	16.8400(1)	17.0335(1)	17.2082(1)	17.3562(1)	17.4346(1)	17.3688(1)	16.7779(1)
V, Å^3	4745.63(2)	4775.55(2)	4942.08(1)	5095.70(1)	5228.38(3)	5299.52(7)	5239.8(1)	4733.94(2)
λ, Å	$CuK\alpha_{1,2}$	$CuK\alpha_{1,2}$	0.35422	0.35422	$CuK\alpha_{1,2}$	0.35422	0.35414	$CuK\alpha_1$
Density	8.088	8.099	8.132	8.188	8.283	8.263	8.369	7.392
2θ range	5–100	5–100	1–30	1–30	8–100	1.9–25	2–25	8–100
Points/refined parameters	7235/43	7235/43	14500/50	14500/52	7007/60	11550/71	14500/67	18460/41
Reflections/ structural parameters	162/21	163/20	467/30	477/33	175/24	304/32	489/28	160/12
				R factors:				
R_F	3.59	2.20	2.22	2.71	2.06	1.39	2.20	2.60
R_P	2.46	1.44	6.35	6.81	0.90	4.81	6.41	4.01
R_{wP}	3.55	2.02	8.39	8.91	1.16	6.17	8.18	5.19
χ^2	2.12	2.42	1.84	1.88	1.77	1.47	1.28	1.31